ACS APPLIED MATERIALS & INTERFACES

www.acsami.org

Research Article

Adhesion of Epithelial Cells to PNIPAm Treated Surfaces for Temperature-Controlled Cell-Sheet Harvesting

Hyejeong Kim, Hannes Witt, Tabea A. Oswald, and Marco Tarantola*

Cite This: *ACS Appl. Mater. Interfaces* 2020, 12, 33516–33529

Read Online

ACCESS | Metrics & More | Article Recommendations | Supporting Information

ABSTRACT: Stimuli responsive polymer coatings are a common motive for designing surfaces for cell biological applications. In the present study, we have characterized temperature dependent adhesive properties of poly(*N*-isopropylacrylamide) (PNIPAm) microgel coated surfaces (PMS) using various atomic force microscopy based approaches. We imaged and quantified the material properties of PMS upon a temperature switch using quantitative AFM imaging but also employed single-cell force spectroscopy (SCFS) before and after decreasing the temperature to assess the forces and work of initial adhesion between cells and PMS. We performed a detailed analysis of steps in the force−distance curves. Finally, we applied colloid probe atomic force microscopy (CP-AFM) to analyze the adhesive properties of two major components of the extracellular matrix to PMS under temperature control, namely collagen I and fibronectin. In combination with confocal imaging, we could show that these two ECM components differ in their detachment properties from PNIPAm microgel films upon cell harvesting, and thus gained a deeper understanding of cell-sheet maturation and harvesting process and the involved partial ECM dissolution.

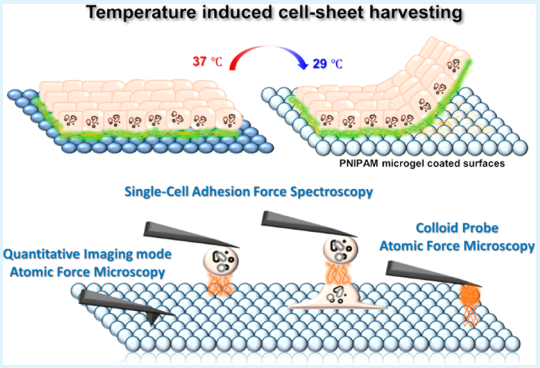

KEYWORDS: *poly(N-isopropylacrylamide) (PNIPAm), cell-sheet harvesting, MDCK II epithelium, atomic force microscopy (AFM), single-cell adhesion force spectroscopy (SCFS), colloidal probe atomic force microscopy (CP-AFM)*

INTRODUCTION

The generation of cell sheets is a milestone in a broad range of biomedical fields, from cell sorting, analysis, confinement, crowding, and differentiation to regenerative tissue engineering of organs, e.g. heart, cornea, skin, or bones.[1−4] Cells are cultured in customized 2D/3D scaffold to suit their needs and transferred to specific wounds or disease sites.[5−7] Often cell adhesion on standard cell culture surfaces is so strong that cell detachment requires a chemical or physical treatment with potentially harmful enzymes or mechanical force.[8] A more gentle approach is controllable cell adhesion on designed substrates in the more unique way of cell-sheet engineering. It fabricates a monolayer of cells and has been described to maintain extracellular structures with minimal damage to the cell morphology and function for tissue reconstruction.[8,9] In clinical applications, cell monolayers have been used to repair ocular trauma by corneal epithelial cell-sheet transplantation.[10,11] To detach the cells efficiently and to minimize the stress on the cells, a variety of synthetic surface coatings with stimuli-responsive adhesion properties has been developed including pH responsive surfaces as well as magnetic or charge/electro-sensitive surfaces.[12,13]

Thermoresponsive polymers with a lower critical solution temperature (LCST) between 25 and 35 °C, such as poly(*N*-isopropylacrylamide) (PNIPAm), are promising candidates for a functional substrate of *in vitro* cell culture substrates.[5,7,14−16] Cell culture substrates functionalized with PNIPAm allow adhesion of a wide variety of cells without the need for modifications to increase biocompatibility like additional cell adhesive ligands or control of substrate stiffness.[17,18] It allows regulation of cell adhesion and proliferation under standard cell culture conditions at 37 °C, while at a temperature lower than the LCST, the surface promotes cell-sheet detachment based on temperature control. Compared with traditional cell detachment techniques such as proteolysis and mechanical scrapping, PNIPAm coated surfaces provoke less damage to the cells and the retention of extracellular matrix (ECM) can be realized, thereby enabling harvesting of complete cell sheets.[19] Therefore, it has been successfully applied to produce many types of cell sheets, for example endothelial cells, cardiomyocytes, or keratinocytes.[9,20−23]

To achieve high efficacy of cell tissue harvesting on the thermoresponsive polymer, a rational surface design of the

Received: May 19, 2020
Accepted: July 6, 2020
Published: July 6, 2020

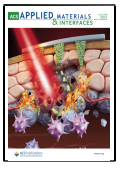

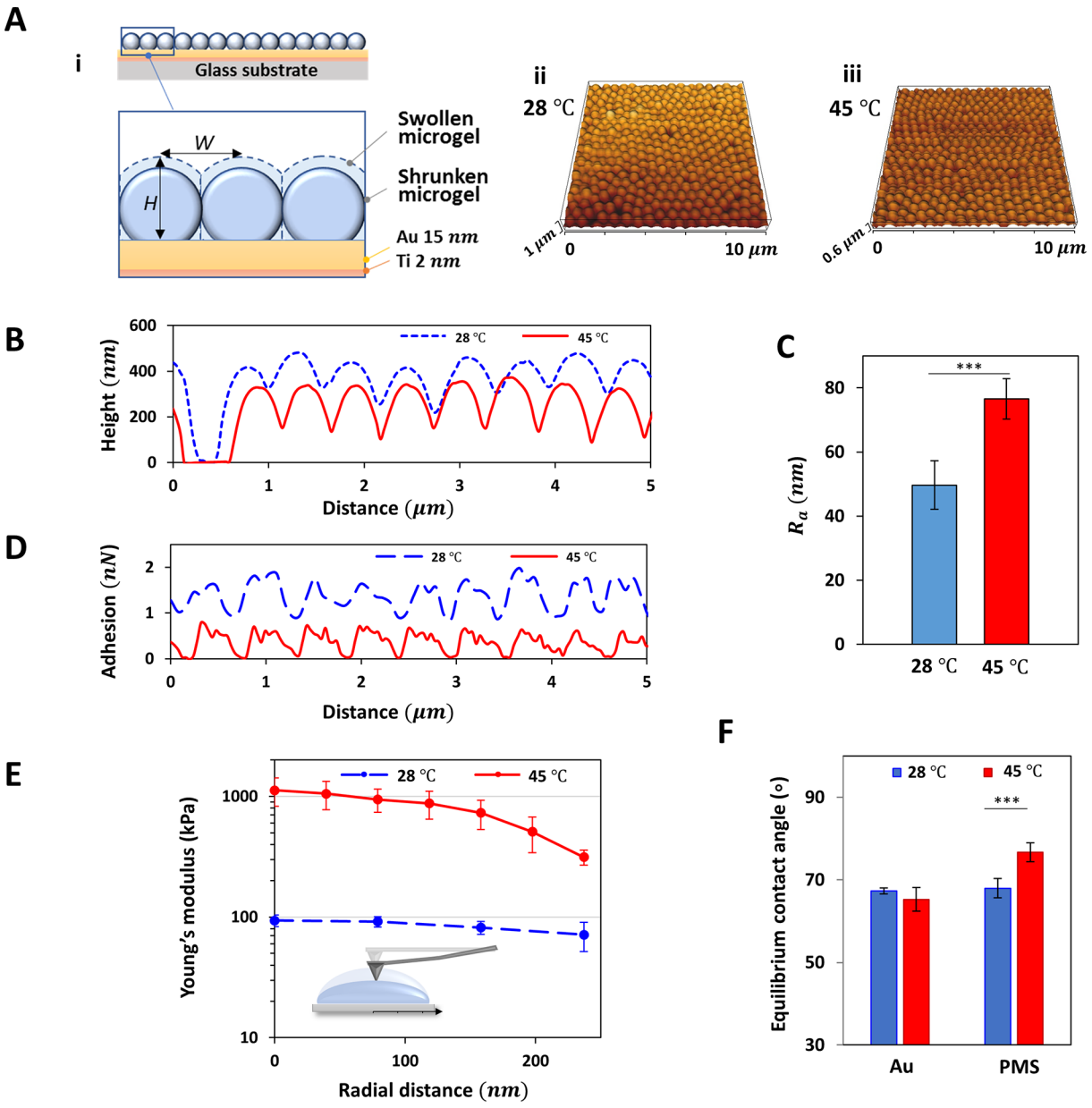

Figure 1. Characteristics of PMS at temperatures below and above LCST. (A i) Scheme with inlet highlighting single PNIPAm-sphere diameter within PNIPAm microgel structure after deposition on gold-coated glass substrate. QI-mode-imaging based topography of microgels at (ii) 28 and (iii) 45 °C. (B) Height of the microgels, *H*, in relation to the gold surface. (C) Average roughness R_a of PMS. (D) Maximum adhesion forces between the cantilever and PMS for a representative scan line. (E) Averaged E-modulus along the radial position from the core of the microgel sphere as shown in the scheme. (F) Equilibrium water contact angles of bare gold surface and PMS at 28 (blue) and 45 °C (red).

culture substrate is required. The effects of surface structure or cell culture duration for optimized cell responses for detaching have been sparsely studied, and the efficacy of cell harvesting appears to vary significantly from study to study in relation to the chemistry, topography, and mechanical properties of the investigated surfaces.[5−7,15,16,24−26] Accordingly, customized polymer surfaces have been designed to suit each target cell-line characteristic. For instance, Yoon et al. developed an elastic piezoelectric substrate based on PNIPAm in order to apply both electrical and mechanical stimuli to skeletal muscle cell sheets.[27] More recently, inspired by marine mussels, a polystyrene surface, layer-by-layer coated with a polydopamine and PNIPAm, has been constructed to culture bone marrow stromal cells.[28]

Even though extensive literature on the properties of the polymer-based coating is available, there is a lack of quantitative investigations considering the influence of the PNIPAm surface on initial cell adhesion[29−31] Additionally, the mechanism allowing cell-sheet detachment from this polymer is still controversially discussed. The most extensive study of the mechanism of detachment proposed a two-step process, with a passive phase involving hydration of PNIPAm chains, and the active phase, involving cellular rearrangements.[32,33] However, Cooperstein et al. reject the two-step hypothesis and imply that the detachment process is predominantly passive suggesting a rapid hydration of PNIPAm chains, which causes the cells to detach from the surface based on unspecific forces.[16] More recently, Switacz et al. found that depending on the size and softness of the polymer, the HEK293T cells could

https://dx.doi.org/10.1021/acsami.0c09166
ACS Appl. Mater. Interfaces 2020, 12, 33516−33529

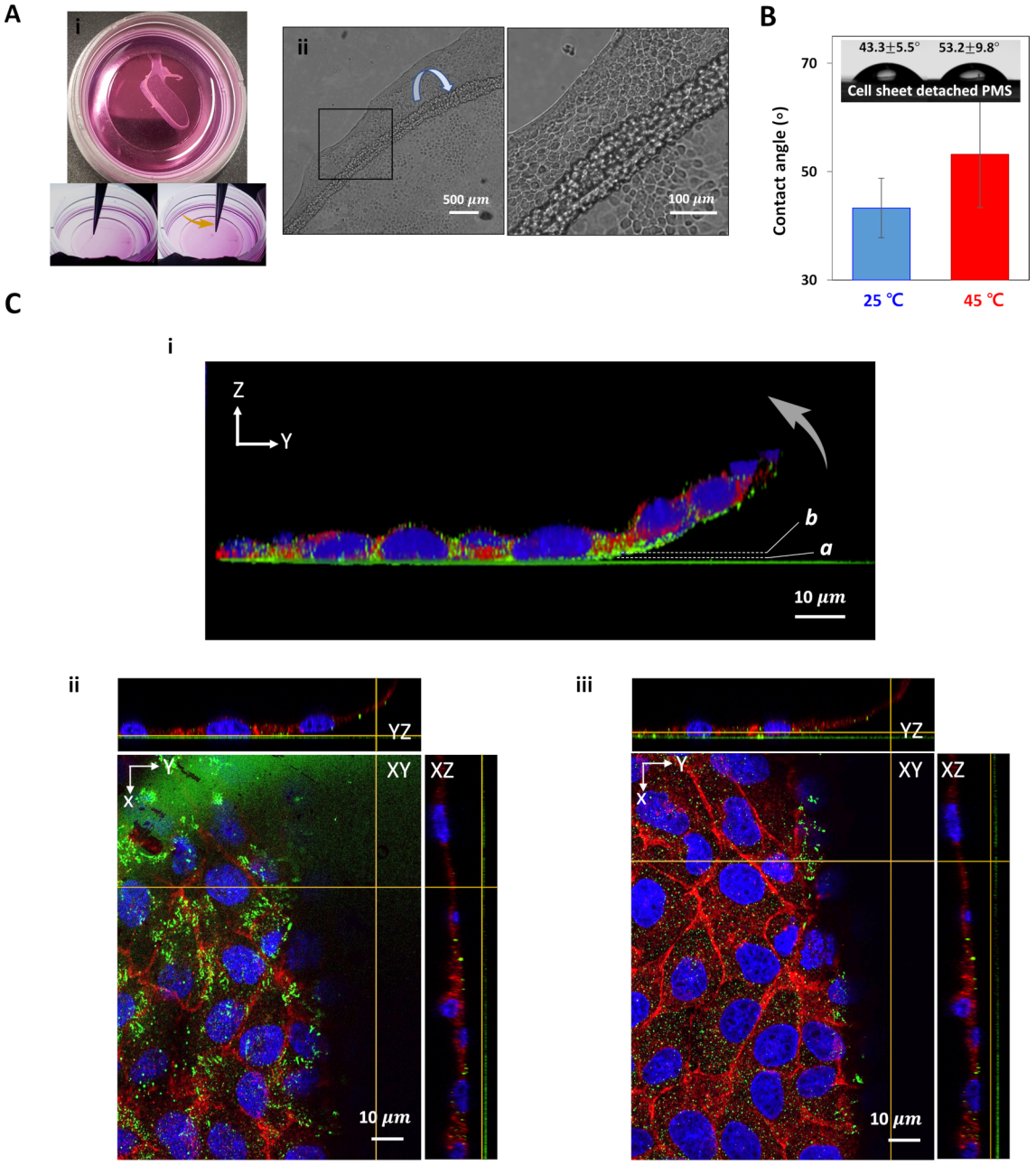

Figure 2. MDCK II cell-sheet harvesting from PMS after 48 h. (A i) Optical images of a gently peeled MDCKII cell sheet and (ii) corresponding phase-contrast images at the rolled-up cell-sheet edge. (B) Equilibrium water contact angles of PMS after cell-sheet peeling at different temperatures below (blue) and above (red) LCST. (C) Confocal images of a fixed MDCK II cell-sheet stained for nuclear DNA (blue), paxillin (green), and e-cadherin (red) on PMS. (i) Merged image of the cell-sheet cross-section upon substrate peel-off (arrow, with a and b highlighting the image plane for parts ii and iii. (ii) Paxillin is well distributed on the ventral surface of the cell sheet at the surface-proximal focal plane *a*. (iii) e-cadherin is distributed between individual cells at the focal plane *b*, e.g. close to the apical cell membrane height.

take up PNIPAm based microgels.[31] Additionally, a correlation of protein adsorption of ECM of cells and the water content of the grafted PNIPAm brushes was investigated.[34] Even though these recent reveals could be the partial determinant for cell-sheet detachment, to fully apply the advantages of functional substrates for cell-sheet harvesting, systematic and consistent evaluation of cell−substrate and cell−cell adhesion on a well-characterized PNIPAm surface is required.[26]

Atomic force microscopy has a four decade spanning history as a method allowing a quantification of material properties and adhesive forces acting between a cantilever probe of varying geometry such as pyramids or colloids and a substrate of choice. The specialized version called single-cell force spectroscopy (SCFS) was established for the characterization of adhesive interactions between cells or between a cell and a model substrate.[35−37] Here, the cantilever tip is replaced by a cell acting as a probe, and thus—in contrast to other methods for cell adhesion studies[38]—it is possible to measure direct adhesive interactions in a minimal invasive fashion down to the pN regime. While AFM has been applied for characterizing PNIPAm properties numerous times,[29,39,40] cell−PNIPAm interactions are only sparsely studied with force sensitive methods.[41,9]

https://dx.doi.org/10.1021/acsami.0c09166
ACS Appl. Mater. Interfaces 2020, 12, 33516−33529

In this study, we explored the mechanism of early epithelial cell adhesion to PNIPAm microgel coated surfaces (PMS). We therefore characterized mechanical properties of PMS such as morphology, adhesiveness, stiffness, and roughness employing quantitative AFM imaging (QI-AFM). These properties, especially the height change of the microgel sphere, are expected to influence early single-cell adhesion cluster dynamics on PMS acting similar to repeller molecules.[41] Therefore, we have quantified cell−substrate adhesive forces by SCFS and step spectroscopy to provide evidence for temperature as well as PMS sensitive contributions to the detachment of unspecific and cytoskeletal-anchored attachment sites. Furthermore, MDCK II cell monolayer formation and its harvesting from PMS were demonstrated, and biomolecules involved in cell adhesion were visualized using confocal imaging techniques. This includes markers for early adhesive junctions to PMS (paxillin)[42] or between cells (e-cadherin) as well as markers for matured epithelia as ZO-1.[43] In addition, colloidal probe atomic force microscopy (CP-AFM) was applied to investigate the adhesive properties of spheres coated either with collagen I or fibronectin, two major components of the fully developed epithelial ECM, to PMS under temperature control. Additional optical characterization showed that upon harvesting collagen I is lifted with the cell sheet as opposed to fibronectin. The results of this study will give us a deeper understanding of the initial cellular adhesive forces and ECM contributions involved in PMS interaction and therefore help to understand the cell-sheet harvesting process, which would be ultimately necessary for designing effective cell culture surfaces in cell-sheet based tissue engineering.

RESULTS

PNIPAm Microgel Films on Gold Surfaces Characterized by AFM Imaging. Since the mechanical properties of the cell culture surface have a huge influence on the initial cell adhesion and cell-sheet detachment from the surface, we quantitatively characterized the mechanical properties of the PMS surface upon temperature variation. When the temperature is reduced to 28 °C, below the LCST, PMS are known to become hydrophilic, increase their water content, and swell. In contrast at 45 °C, which is above the LCST, the microgels become hydrophobic, reduce their water content, and deswell, thus collapsing, which affects the micrometer scale structure as well as the mechanical properties of the PMS and its surface. We used gold surfaces noncovalently coated with PNIPAm microgels, because of the biocompatibility of the surface and stable adhesion without additional chemical treatment. The morphological and mechanical characteristics of PMS were measured by quantitative AFM imaging at 28 and 45 °C (Figure 1A). The microgel spheres are homogeneously distributed on the surface with rare holes in the regular lattice structure indicating defects or occasional single sphere liftoff (Figure S1, S2). As temperature decreases from 45 to 28 °C, the average height of the microgel from the bottom, H, increases from a mean ± SD of 327 ± 12 to 400 ± 27 nm while the distance between adjacent microgels, W, is almost unchanged (558 ± 25 to 547 ± 45 nm), which indicates that within the tightly packed monolayer the volumetric changes of the microgels mainly occur in vertical direction without large rearrangement in radial direction (Figure 1B). The arithmetic average roughness R_a is almost 1.5 times higher when the microgels shrink above the LCST (R_a = 76.5 ± 6.3 nm) than in the swollen state (R_a = 49.7 ± 7.6 nm) (Figure 1C). Furthermore, unspecific adhesion forces between the cantilever and the PMS increase upon temperature reduction (Figure 1D) from 0.5 to 1.5 nN maximal adhesion force. The elastic modulus E for the collapsed state is significantly higher than for the swollen states. The core of the PNIPAm microgel has the highest E-modulus, which decays radially outward (Figure 1E). When collapsed, the E-modulus of the microgel widely varies from around 1.1 MPa (at the middle of the PMIPAm microgel) to 310 kPa (at the periphery). When the microgel swells due to cooling, the values strongly decrease to 93 kPa at the core and 71 kPa at the periphery. Therefore, the central part of the microgel decreases its stiffness by almost 12 times, while an almost 4-fold decrease is detected near the edge of the sphere. Contact angle measurements, which relate to the wettability of the surface, show that the PMS at 45 °C yields a higher degree of hydrophobicity, as indicated by the increased static water contact angle (SCA), while the wettability of the gold surface does not change significantly with temperature (Figure 1F, S4). In summary, while the height increase of the microgels is very prominent, we find a reduced roughness, an increased unspecific adhesiveness, a reduced stiffness, and an increased hydrophilicity upon temperature reduction below the LCST, and therefore, no trend allowing a clear prediction on how these changes influence cell adhesion, necessitating a thorough study of cell−substrate adhesive forces as well as a functionality of the PMS induced cell-sheet harvesting.

Cell-Sheet Harvesting from PMS after 2 Days of Culture. Homogeneous monolayers of PMS were prepared and characterized as described above, and MDCK II cells were seeded onto the substrate in full cell culture medium and incubated at a temperature of 37 °C. Inoculum density was chosen to provide a monolayer cell sheet after 48 h of incubation (please refer to Figure S9 for 6 h morphology). To demonstrate the PMS functionality, we cooled the culture down to 25 °C, where cell sheets detached from the surface and could be removed by gentle peeling at the sheet (Figure 2A). The SCA values of PMS, from which the cell sheet has been detached, are smaller than those of the bare PMS, which indicates that some hydrophilic components of the cell sheet remain attached to the PMS. This limits multiple usage, as also the temperature responsiveness of the substrates is not fully retained (Figure 1F, 2B, S4).

As mechanics and dynamics of the epithelial cell sheets are strongly dependent on the presence of cell−cell and cell−substrate adhesion contacts, we furthermore analyzed their integrity upon PMS based thermosensitive detachment from the surface via immunofluorescence. The focal adhesion protein paxillin and the cell−cell adhesion protein e-cadherin were visualized using confocal imaging (Figure 2C). The MDCK II cell sheets grown on the PMS show comparable morphology to that observed on control gold substrates (Figure S3), which were used to cast PNIPAm microgel films.

When the cell sheet was detached from the substrate with the help of the temperature decrease after 48 h of culture, paxillin punctae with varying size distribution indicating partial focal contact maturation are detached together with the cell sheet (Figure 2Ci, ii), hinting at intact basal membranes. As we also detected continuous e-cadherin staining between the cells, the temperature induced PMS cell-sheet lifting retained cell−cell adhesions (Figure 2Ci, iii), thus demonstrating the noninvasive detachment procedure and formation of a viable cell sheet. In conclusion, we were able to successfully create

https://dx.doi.org/10.1021/acsami.0c09166
ACS Appl. Mater. Interfaces 2020, 12, 33516−33529

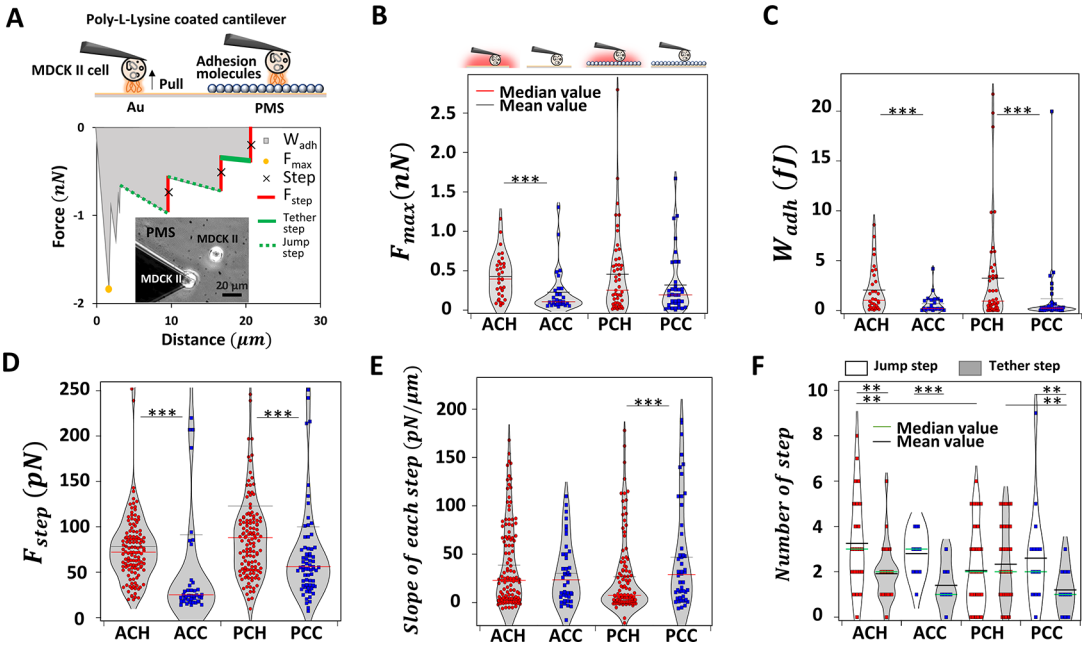

Figure 3. Cell adhesion on bare gold and PMS upon temperature changes monitored via SCFS. (A) Schematic overview of AFM-based cell−substrate adhesion experiments (top). Representative force−distance curve and the corresponding general adhesion as well as step analysis of a single MDCK II cell on PMS. Determined parameters F_{max}, W_{adh}, F_{step}, number of steps, and step slope are highlighted and color coded (bottom). Bright field image of the cantilever tip with an attached single MDCK II cell while recording cell−substrate adhesion force curves and a second surface-attached cell (inset). F_{max} (B), W_{adh} (C), step force F_{step} (D), step slope (E), and number of jump steps and tether-like steps (F) of MDCK II cells on gold substrates and PMS, all upon temperature switch, corresponding categories schematically given at the top (red or green line median value; black line mean value). ACH/ACC for Au−cell interactions at heated/cooled states; PCH/PCC for PMS−cell interactions at heated/cooled states; respectively. A significance test is only shown for temperature changes; for all additional categories, refer to Figure S13 and Table S5.

cell sheets already after a two day culture on PMS by temperature-induced liftoff, preserving cell junctional integrity.

Early Cell−Substrate Adhesion on PMS upon Temperature Changes Monitored via SCFS. We next studied the initial cellular adhesion within seconds to minutes on PMS in detail, especially regarding forces of adhesion and the corresponding adhesion work needed to detach cells from PMS. We quantified the biomolecular interaction between the cells and the PMS regarding cell−substrate interactions at 30 s contact times. For additional results on cell−cell adhesion after 30 and 90 s contact times, refer to supplementary chapter S1, Table S1, and Figure S7, where also the first significant PMS based modifications could be observed.

We performed AFM based SCFS experiments at temperatures above and below the transition temperature (schematically shown in Figure 3A, top). Each case is labeled as follows: ACH/ACC for gold−cell interactions at heated/cooled states; PCH/PCC for PMS−cell interactions at heated/cooled states (see Figure S5 for exemplary micrographs). Direct cell adhesion measurements were carried out by first picking single MDCK II cells from the gold substrate using a tipless cantilever functionalized with poly-L-lysine and then performing the actual measurement either on the PMS or a different position of the gold substrate. The maximum force of adhesion F_{max} serves as a measure of general unspecific adhesion upon detachment, while the work of adhesion W_{adh} is as a parameter also sensitive to the strength of specific adhesions and adhesion clusters interacting with the surface.[25]

To extend, we performed a detailed analysis of steps in the force curves (Figure 3A, bottom): the retrace part of a typical SCFS force-distance (FD) curve shows several local minima appearing in a step-like fashion, which can be attributed to rupture of cytoskeletal-anchored adhesion sites (here referred to as jumps, dotted lines in green in Figure 3A) and pulling of membrane tubes from the cell membrane (referred to as tethers, solid green lines in Figure 3A) as also described previously.[44,45] Within the step analysis presented here, we analyzed the total number of steps, their step force F_{step}, the step length l_{step} between two steps, and the distance to the underlying substrate needed to completely detach the cell (pulling length $l_{pulling}$); for all additional categories, refer to Figure S13 and Table S5. We furthermore determined the slope between steps to distinguish jumps from tethers and calculated the ratio of these two specimens (Figure S9). Table 1 summarizes all results in terms of median and mean results including the degree of changes for the temperature reduction on PMS and reference gold substrates. Please refer to supplementary chapter S1 for corresponding results on cell−cell adhesion and to Figure S6 for a selection of representative FD curves as well as Table S6 for an overview of independent experiments, cells, and FD curves employed.

First, we monitored the maximal adhesion forces F_{max}, and surprisingly adhesion forces did not change on PMS above and below the LCST. We can observe adhesive forces ranging from 0 to 3 nN (Figure 3 B), with a slight decrease of F_{max} from the heated to the cooled state on gold. W_{adh} reflects continuum and stochastic parts of cell unbinding and is summarized in Figure 3C: reducing the temperature below the LCST leads to significantly reduced adhesion energies for both gold substrate and PMS. W_{adh} was thus more sensitive than F_{max}, and the adhesion work decrease could be either mediated by the PMS or only be a temperature effect. Therefore, we now focused on the contributions of steps to the adhesion process. We distinguish between tethers (value of slopes is ≤10 pN/μm)

https://dx.doi.org/10.1021/acsami.0c09166
ACS Appl. Mater. Interfaces 2020, 12, 33516−33529

Table 1. F_{max}, W_{Adh}, F_{step}, step slope, l_{step}, N_{step}, and $l_{pulling}$ for SCFS Based Cell Liftoff from PMS and Gold Substrates above and below the LCST, Given as Mean (M), Standard Deviation (SD), Median (MD), and Degree of Change

		ACH	ACC	PCH	PCC
F_{max}	mean, M, (nN)	0.43	0.23	0.46	0.32
	M(C)/M(H) (%)		53		70
	SD (nN)	0.28	0.29	0.53	0.39
	median, MD (nN)	0.39	0.11	0.25	0.19
	MD(C)/MD(H) (%)		27		76
W_{adh}	M (fJ)	2.04	0.68	3.23	1.16
	M(C)/M(H) (%)		33		35.8
	SD (fJ)	2.30	0.93	5.17	3.47
	MD (fJ)	1.02	0.19	0.93	0.22
	MD(C)/MD(H) (%)		19		24
F_{step}	M (pN)	78.29	91.27	122.87	99.89
	M(C)/M(H) (%)		116.6		81.30
	SD (pN)	43.29	146.76	184.07	148.62
	MD (pN)	72.10	25.00	88.05	56.00
	MD(C)/MD(H) (%)		34.67		63.60
slope	M (pN/μm)	38.67	30.39	26.72	46.89
	M(C)/M(H) (%)		78.58		175.5
	SD (pN/μm)	44.54	32.72	40.55	56.41
	MD (pN/μm)	23.00	23.50	7.50	29.00
	MD(C)/MD(H) (%)		102.2		387
L_{step}	M (μm)	2.31	1.78	4.36	3.62
	M(C)/M(H) (%)		77.1		83.1
	SD (μm)	3.58	4.11	8.47	5.92
	MD (μm)	1.08	0.44	1.14	1.31
	MD(C)/MD(H) (%)		40		115
N_{step}	M	3.97	2.58	3.09	2.21
	M(C)/M(H) (%)		65.0		71.6
	SD	3.37	2.80	3.17	2.91
	MD	3	3	2	1
	MD(C)/MD(H) (%)		100		50
$L_{pulling}$	M (μm)	10.34	6.51	15.61	10.80
	M(C)/M(H) (%)		62.9		69.20
	SD (μm)	9.04	10.55	21.11	15.78
	MD (μm)	8.41	2.21	4.61	2.53
	MD(C)/MD(H) (%)		26.2		54.9

and jumps (slopes >10 pN/μm). Slope values higher than 200 pN/μm (mostly appearing in vicinity to F_{max}) were rejected; not all force curves show steps, some presenting only unspecific peaks quantified via F_{max}, please compare Tables S2 and S6 for the number of force curves used for step analysis. As shown in Figure 3D, the forces per rupture event F_{step} are significantly decreased on gold and PMS upon cooling, the latter generally showing higher F_{step} at both temperatures (see also Figure S13E). The total number of steps N_{step}, the total distance needed to separate cells from the substrate $l_{pulling}$ and the length of force plateaus between ruptures l_{step} are all independent of the temperature switching (Figure S13C, D, and G). However, the slopes of FD curves just before a step show a specific PMS effect beyond a merely temperature-based reduction as summarized in Figures 3E and S13F: temperature reduction leads to a significant step slope increase only on PMS. By analyzing all slopes cumulatively and determining the number and ratio of jumps and tethers (Figures 3F and S8 but also compare supplementary Figures S9 and S10 as well as Tables S2–4 on the absolute step number), we furthermore see that, while on gold the ratio is temperature invariant with a slight shift to tethers, on PMS the occurrence of jumps shows a 3-fold increase.

We can therefore conclude that reducing the temperature leads to an absolute increase of jumps to tether ratio (e.g., jump amount slightly increases while tether amount decreases) on PMS and only a relative increase on gold (only the amount of tether decreases), allowing the statement that the cells switch to cytoskeletal attachment upon adhesion to cooled PNIPAm as compared to having more unspecific attachment via membrane tether at higher temperatures or on gold.

Given this is very early interaction to PMS, we however need to ask the question how the interaction of fully developed epithelia with a mature ECM is affected by the PMS culture.

ECM–PMS Interaction Studied by CP-AFM and Cell-Sheet Harvesting after Prolonged Cell Culture. For the majority of cells, ECM proteins are the main interface precursor to cell attachment mediating the biomaterial–cell interaction. Here, the adhesive interaction between two major components of the ECM, collagen I and fibronectin, and the synthetic PMS are characterized as a function of temperature changes. Fibronectins are fibrillar glycoproteins that provide cell-surface integrin with RGD motives for binding and collagens I and IV are the most abundant proteins present in the ECM that give structural support to resident cells, either forming stiff or soft, gel-like matrices.[46] Full epithelial sheet development furthermore relies on cell–cell contacts for the mechanical stability of epithelial tissues. In epithelia cells, besides gap junction communication contacts, adherens junctions based on cadherins can serve as belt-like structures creating a mechanical, tissue-spreading continuum linked to catenins and actin. They also serve as a necessary prerequisite for tight junction formation.[43] The latter represent an apical diffusion barrier controlling paracellular permeability. They are composed of claudins, JAM, or occludins in the intercellular gap, themselves connected to the actin cytoskeleton via various zonula occludens (ZO) linkers in the cytoplasm, which in their scaffolding function mediate communication and growth impulses from adherens to the gap and especially tight junctions.[47] Here, confocal microscopy was used to analyze the ZO-1 presence. Furthermore, CP-AFM was used to investigate the intermolecular interaction between the ECM proteins coated on the spherical probe and PMS above and below the LCST.

We analyzed F_{max} and W_{adh} from typical FD curves. The median F_{max} of fibronectin on PMS increased from 0.5 to 0.8 nN as the temperature decreases from 37 to 29 °C, whereas it decreases on the gold surface from 0.6 to 0.5 nN (Figure 4A). W_{adh} shows an increase for fibronectin on both gold (from a median of 1 to 1.5 fJ) and PMS (from a median of 0.6 to 1.4 fJ) with the temperature decrease (Figure 4B). Confocal images visualizing fluorescently tagged fibronectin of cell culture on PMS for 1 week reveal that the fibronectin is present not only under the cell sheet before temperature switching but also below the area where the cell sheet is still attached as well as where the cell sheet has been peeled off from the surface (Figures 4C and S8). Here, after 7 days of culture, tight junctions have been formed as can be seen by the continuous ZO-1 staining and also the ECM is homogeneously distributed over the PMS surface, thus comparable to the CP-AFM approach.

On the other hand, collagen I shows a decreasing median F_{max} on PMS from of 0.09 nN to 0.05 nN) while on gold F_{max} varies nonsignificantly between 0.09 and 0.1 nN upon

https://dx.doi.org/10.1021/acsami.0c09166
ACS Appl. Mater. Interfaces 2020, 12, 33516–33529

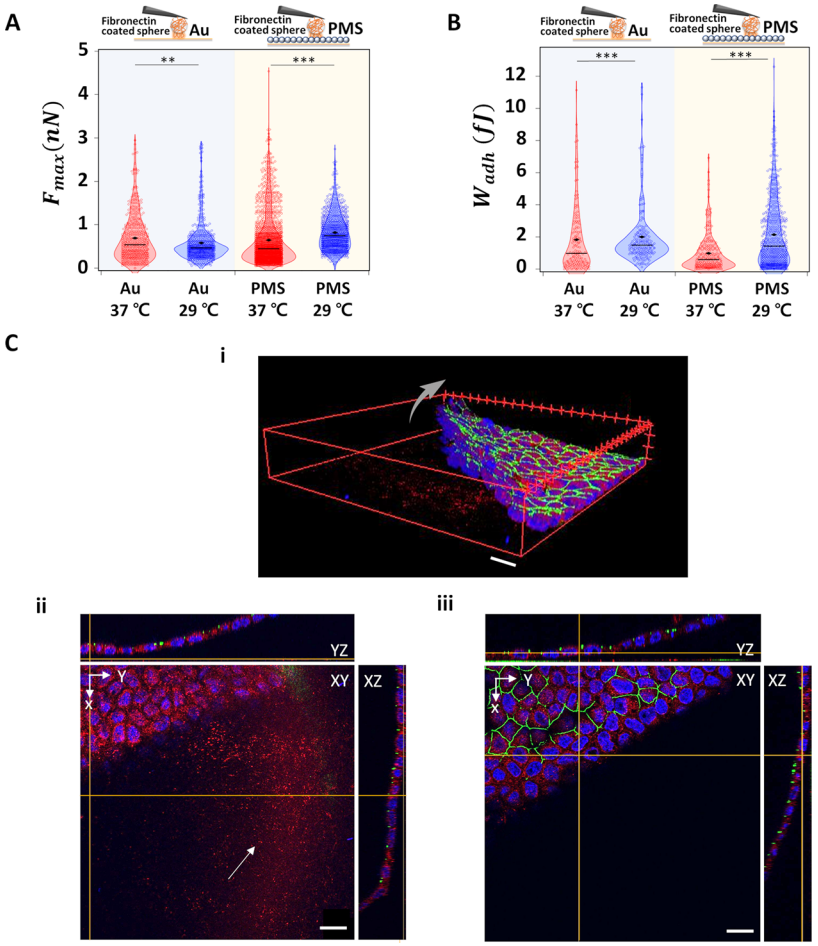

Figure 4. Interaction between ECM component fibronectin and gold or PMS. (A) F_{max} and (B) W_{adh} of colloidal, fibronectin coated AFM cantilever to the gold substrate and PMS upon temperature switching (— median value; ◆ mean value). (C) Confocal images of 1 week cultured MDCK II cell sheet, thereupon fixated and stained for nuclear DNA (blue), ZO-1 (green), and the ECM component fibronectin (red) on the PMS. (i) 3D image of the detaching cell sheet from 7 days culture on PMS (arrow). (ii) Corresponding staining to i, with focus on substrate plane; remnant PMS-attached fibronectin highlighted (arrow). (iii) Corresponding to i, focal plane on apical cell membrane height: staining of tight junction protein ZO-1 is continuous between the cells. Scale bar: 20 μm. Significance test only shown for temperature changes; for all additional categories refer to Figure S14 and Table S5.

temperature reduction (Figure 5A). W_{adh} shows a decrease for collagen I on both gold (median of 0.011 to 0.001 fJ) and PMS (median of 0.01 to 0.004 fJ) with temperature decreases (Figure 5B). Both parameters are 1 order of magnitude smaller than for fibronectin. The confocal images for 7 days old cultures show—besides continuous ZO-1 distribution—that collagen does not remain attached on the polymer surfaces after the cell sheet is lifted upon temperature decreases (Figure 5C). Additional measurements at 45 °C confirm this trend and are shown in Figure S10. Overall, fibronectin and collagen I, though both ECM building blocks, show opposite behavior upon cell detachment, which indicates that the differential adhesion after 7 days of culture between ECM components and the PNIPAm microgel films as well as tight junctions' presence could contribute to cell-sheet harvesting; this duality might be a consequence of the PMS ability to swell and thus induce a water withdrawal from the fibrillar ECM hydrogels.

DISCUSSION

In the present work, we have quantified several aspects relevant to cell-sheet harvesting using PMS: mechanical properties of the surface including the morphology, adhesion, roughness, Young's modulus, and contact angle were assessed using QI-AFM. We furthermore studied three different time scales relevant to PMS−biointerface interactions: (1) initial cell−substrate as well as cell−cell interaction within seconds to minutes using SCFS, (2) cell-sheet detachment from 6 h to 2 days of culture including the study of markers for focal− and cell−cell contact maturation, and (3) cell-sheet harvesting after extended culture of 1 week including the screening for mature epithelia via ZO-1 imaging and relevant ECM contributions applying CP-AFM.

Regarding the PMS characterization, the height of single microgel spheres increased by a factor of 1.3 based on AFM imaging. It then shows a truncated, symmetric sphere for the microgel in the swollen, cooled state. This size increase is accompanied by an unspecific adhesion force increase, and the latter could be linked to the increased surface area and changed number of free polymer chain ends on the surface interacting with the AFM tip and thus based on van der Waals forces, as has been also hypothesized elsewhere.[39] We monitored the roughness of the PMS which shows a decrease of R_a from 76 to 49 nm with temperature reduction; this matches previous literature for PMS.[48] Interestingly, this also matches feature spacings found for integrin maturation (<60 nm).[49,50]

https://dx.doi.org/10.1021/acsami.0c09166
ACS Appl. Mater. Interfaces 2020, 12, 33516−33529

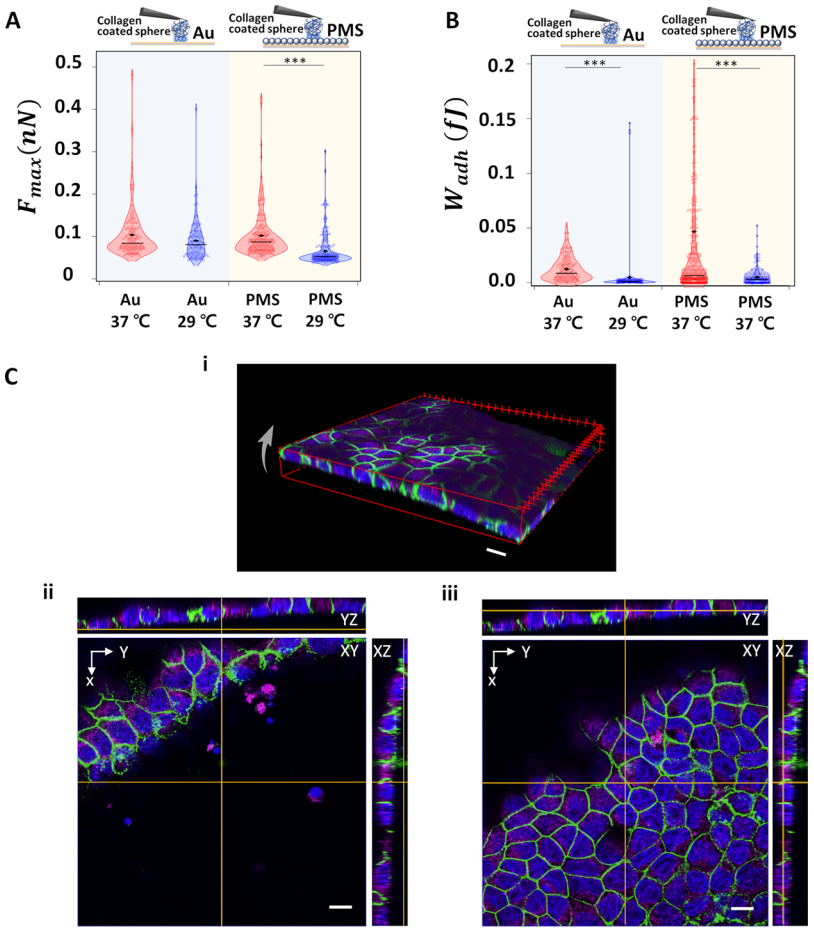

Figure 5. Interaction between ECM components collagen I and gold or PMS. (A) F_{max} and (B) W_{adh} of colloidal, collagen-coated AFM cantilever to the gold substrate and PMS upon temperature switching (— median value; ◆ mean value). (C) Confocal images of MDCK II cultured for 1 week and cell sheet fixed and stained for nuclear DNA (blue), ZO-1 (green), and collagen 1 (magenta) after 7 days of culture on the PMS. (i) 3D image of the detaching cell sheet from the substrate (arrow). (ii) Corresponding staining to i, with focus on substrate plane: collagen I rarely remains attached to PMS. (iii) Corresponding to i, focal plane on apical cell membrane height: staining of tight junction protein ZO-1 is continuous between the cells. Scale bar: 10 μm. A significance test is only shown for temperature changes; for all additional categories refer to Figure S14 and Table S5.

Moreover, substrate stiffness matters for cell adhesion, as mammalian cells prefer to adhere to substrates with E-moduli of comparable or higher strength up to a limit of 50−100 kPa.[17] It is believed that the physical mechanism of substrate rigidity sensing by a cell is the assessment of the substrate deformation resulting from the traction forces exerted by the cell. The heated, collapsed PMS with elasticities of 310 kPa−1.1 MPa is thus perceived as infinitely rigid similar to some specialized ECMs (elasticities *in vivo* ranging up to MPa/GPa[51−54]). The swollen PMS however reaches elasticities of 71−93 kPa and thus 1 order of magnitude above the ones of MDCK II cells (5−10 kPa[55]). This elasticity lies within the stiffness detection regime, and therefore, the reduced rigidity of the cooled PMS might effect adhesion. However, durotaxis can be excluded due to small sphere sizes and therefore missing spatial stiffness gradient extension. Similar effects for E-moduli decreases of microgels were also described before, quantified over the whole range from 45 to 25 °C and found to accompany volume and water content increase.[39] We also found the contact angle to significantly decrease with temperature when PMS is expected to become more hydrophilic. In the literature, increasing the hydrophilicity of surfaces did not lead to increased MDCKII attachment efficiency.[56] Therefore, the height increase of the microgel spheres should influence membrane height and thus bending and adhesion bond clustering and decrease adhesion, but the roughness decrease should favor adhesion. Furthermore, unspecific interactions based on area increase and thus mainly on van der Waals forces should lead to increased adhesion, while stiffness changes are not expected to impact adhesion strongly. Along the same lines the increase of hydrophilicity should have only a minor impact on adhesion.

Since the sole mechanical characterization of the substrates did not lead to a clear prediction regarding temperature dependent cell−substrate adhesion on PMS, we now focused on SCFS, which for the cell−substrate adhesion is reported to rely on integrins. MDCK possesses heterodimeric integrins from the β1 family like $\alpha_2\beta_1$, $\alpha_3\beta_1$ for the interaction with collagens I and IV as well as laminin, while β3 integrins like $\alpha_v\beta_3$ are used for general RGD based multisubstrate adhesion, e.g. to fibronectin or vitronectin, while they also control collagen specific focal contact maturation including talin recruitment.[57] Additionally, $\alpha_6\beta_4$ heterodimers have been described in 3D culture growth interactions.[58,59] Regarding integrin kinetics, studies on $\alpha_2\beta_1$ integrins in CHO cells showed that extended contact times above 60 s show signs of

https://dx.doi.org/10.1021/acsami.0c09166
ACS Appl. Mater. Interfaces 2020, 12, 33516−33529

cooperativity, bond clustering, and actomyosin dependence.[36] Recently, specific integrins of the $\alpha_5\beta_1$ family possessing catch bond behavior were shown to even have activation times below 1 s.[60] We decided to use 30 s contact times to focus on the initial interaction of MDCK II cells with PMS and thus negligible ECM deposition by the cells. Our results showed that F_{max} is not significantly affected by temperature decrease as opposed to W_{adh}. We expect α_v or α_5 integrin bonds or bond clusters to mediate these early effects and α_2 based clusters at later stages, which could be confirmed in the future using specific antibody-based inhibition. Note that we, however, did not observe spontaneous lifting of individual cells at this stage. We also found a significant temperature based reduction in W_{adh} for the establishment of early cell−cell contacts with 90 s contact times (see supplementary chapter S1). Cell−cell adhesion forces determined here upon thermoresponsive behavior of the coating represent PNIPAm based modulation of initial cell−cell adhesion based on early junctional contacts of the surface attached cell, mainly mediated through the dynamics of cadherines. They are not indicative of the confluent situation where all interacting cells had extended contact to PMS and multiple junctions with their neighbors as well as a fully developed ECM/focal contacts interface. De facto only the surface attached cells' reaction to the PMS in terms of junction dynamics is probed against another cell in contact to the cantilever functionalization,. As such these forces were however also compared to bare temperature drop effects to identify significant deviations from the situation, where one cell attached to poly-L-lysine and the other cell to gold (please refer to significance test in the subfigures of supplementary Figure S13, especially categories with green-labeled background referring to the 90 s contact time). Therefore, the culture on PNIPAm is also affecting early interactions between the cells. Due to the dwell time, these should rely on individual bonds and clusters of e-cadherins, which can form within 1−2 min.[61−63]

When analyzing steps in the FD curves, we found F_{step} of 50−100 pN for cell−substrate contacts and 30−70 pN for cell−cell contacts. Previous AFM based step spectroscopy work has described F_{step} medians of 90 pN for integrins at comparable contact times/forces/pulling length[57] and for single e-cadherins, rupture events of 25 pN were described,[64] while 50−100 pN could be explained assuming initial cluster formation.[65] The main surprising SCFS result in our work, however, stems from the step slope spectroscopy: the prevalence of jumps as opposed to tethers, especially for the cell−substrate adhesion. For the force curves used for step spectroscopy, we found that reducing the temperature leads to an absolute increase of jumps to tether ratio on PMS and only a relative ratio increase on gold, allowing the statement that the cells switch to cytoskeletal attachment upon adhesion to cooled PNIPAm as compared to having more unspecific attachment via membrane tubes at higher temperatures or on gold. Tether seem even slightly more prominent on PMS at high temperatures as compared to gold, so that in summary cytoskeletal anchoring seems more material-sensitive and tether more temperature-sensitive. What could be a mechanism explaining these results? If we roughly compare the ventral area of an adherent but not fully spread MDCKII cell and the microgel spheres, we can easily assume tens to hundred PNIPAm microgel spheres below one cell (see also Figure S5). Initial adhesion was previously assumed to rely on 10 000 individual adhesion bonds, so we basically speculate that each microgel sphere has roughly 25−100 bonds on its surface and later forms one or only a few clusters, which also matches current research findings: taking into account new progress in high-resolution imaging, it is accepted that an integrin cluster should be of 80−120 nm in size incorporating 25−50 molecules, or—for cadherin clusters—50−650 nm sized, containing 10−120 molecules.[66] We therefore expect that swelling of the spheres directly influences the height of the ventral cell membrane, thus the distribution of areas with close or remote proximity to the substrate. The PNIPAm spheres could act similar to an increase in repeller molecules sticking out of a membrane (big steric repeller molecules typically are glycocalyx components), which also energetically favor clustering of adhesion molecules in domains of close substrate vicinity and thus might explain the increase in jumps.[41] Finally, when we compare cell−cell to cell−substrate adhesion, F_{max} and W_{adh} are similar in magnitude and F_{step} is even lower for the latter. Therefore, cell−substrate attachment to the polymeric surface prevails over cell−cell interactions in this early adhesive state.

After extended MDCK II culture of 6 to 48 h on PMS, we can clearly see optical markers for the maturation of the focal contacts such as paxillin as well as markers for adherens junctions and thus cell−cell coupling, here e-cadherin. Temperature switching below LCST allows a cell-sheet liftoff and confirms PNIPAm microgel functionality also against degradation or sphere internalization/endocytosis. Changed contact angles reveal that hydrophilic material, presumably remains of the ECM, is left on the PMS surface, limiting reuse of the substrate (Figure S4). Other studies used phases of 20 min below LCST to lift subconfluent L929 fibroblasts from PNIPAm microgel films after 48 h of culture.[39] On PNIPAm brushes, force quantification for 24 h was shown to yield F_{max} values 2 orders of magnitude higher than the ones described in the present study (above LCST), and temperature reduction led to a decrease to 10 nN.[9] As we are dealing with confluent but not overconfluent densities of MDCK II cells after 48 h, the height increase of the PNIPAm film upon temperature reduction might not only serve as an adhesion repeller but actually activate mechanosensitive signaling feedback loops as described for paxillin/talin or cross communication from cell−substrate to cell−cell contacts via α catenin and vinculin.[67] This also highlights the benefit of PMS usage, as vinculin was shown to be preserved when using PNIPAm for subculture over mechanical or chemical dissolution.[8] Thus after 48 h and in contrast to the early adhesion phase, cell−cell contact forces based on cadherins should dominate this culture phase.

After 1 week of culture, confluency on PMS is also achieved for low initial cell inoculi, and the presence of tight junction protein ZO-1 clearly confirms further cell-sheet differentiation. Cross-communication between all three junction types can be mediated by ZO scaffolds and for example occur via the cytoskeletal signaling, but also through regulating membrane composition[68] or cortical tension,[69] which all could be influenced by PMS culture. We furthermore expected now full surface coverage of PMS by ECM, which could be confirmed optically. This motivated further cell-free studies with dense fibronectin or collagen I coatings in a colloidal probe AFM fashion: fibronectin showed higher and collagen I lower adhesiveness to the PMS below LCST, and F_{max} as well as W_{adh} are 1 order of magnitude lower in the latter case, matching the work of adhesion described by Schmidt et al.[39] We also showed via immunofluorescence microscopy that

https://dx.doi.org/10.1021/acsami.0c09166
ACS Appl. Mater. Interfaces 2020, 12, 33516−33529

collagen I detachment occurs upon cell-sheet harvesting in cell cultures on PMS after 1 week of culture, while this is not the case for fibronectin. While electrostatics could influence protein adsorption here,[70] we expect van der Waals forces to become shielded by ECM and this effect to reduce unspecific adhesion. As we have a three layer system (PMS−ECM−cell), another main contribution to the reduction of cell adhesion upon temperature decrease might be ECM dehydration. Previous literature has also shown destabilization of collagen 1 and fibronectin fibers on PNIPAm substrates.[28] This ECM dehydration could be induced by water uptake through the swelling PNIPAm, and ECM adsorption on the PMS or the detachment of the cell layer would then be based on the stability of each ECM component against loss of water. This should be less influential for fibrillar components than gel-like matrices.

Future PMS based cell-sheet harvesting studies should focus on the late culture phase of MDCK II sheets on PNIPAm after several days of culture and matching techniques like pipet aspiration,[71] impedance spectroscopy,[72] or FluidFM. Especially the latter provides increased liftoff forces needed for detachement of individual cells out of a confluent environment using a hollow cantilever and negative pressure to bind the cells to the tip. FluidFM technologies have been shown to detect 2−3 orders of magnitude higher F_{max} forces in dependence on cell−cell contacts when lifting single cells out of cell sheets as compared to SCFS and in comparison to subconfluent, single cells.[73,74] Therefore, it might be ideally suited to measure the strength of cell−cell contacts above and below the LCST after monolayer formation, and we could already provide a first evidence that cell−cell adhesive forces are PMS modulated for subconfluency here. As cadherines and not ZO-1 were shown to control MDCK II cell mechanics, it would also be worthwhile to study the cortical tension and area compressibility for PMS cultured MDCK II cells[69] and also for all stages of cell confluency to account for stiffness changes and tension homeostasis upon transition to crowding.[75] Finally, further ECM components need to be studied to understand the whole range of cell−ECM−PMS interactions, for example by using micropatterned ECM substrates[76,77] on PNIPAm including also collagen 4, vitronectin, laminin but also specific integrin antibody inhibition studies to get a grasp on the differential adhesion profile of multiple involved integrins in PMS adhesion.

In summary, our working hypothesis is that driving forces for the cell-sheet liftoff from the PMS are depending on the cell culture stage and the presence of corresponding cadherins and tight junctions for cell−cell interactions. For early cell−substrate interactions, the PMS might act directly as a repeller inducing bond segregation into cluster and adhesion strengthening upon temperature decrease, also depending on the cell-specific integrin portfolio. Subsequently, maturation of the cell−substrate and especially cell−cell contacts as well as the increased ECM production matter: unspecific attractive cell−substrate interactions to the PMS are decreased due to continuous ECM covering the PMS. Furthermore, the latter is destabilized by dehydration, so that the cell−substrate forces are overcome by cell−cell adhesion forces and lead to the detachment of a cell sheet.

CONCLUSION

AFM based QI mode imaging, which allowed for a detailed characterization of thermoresponsive PMS such as surface roughness, elastic modulus, and adhesiveness, and also additional wettability studies were carried out below and above LCST, with all parameters showing temperature dependence, although some favoring and some reducing the predicted cell adhesion. Adhesion forces were thus quantified based on SCFS for early cell−PMS interaction and allowed no distinction of these driving forces upon temperature switching, while adhesion energies and thorough step spectroscopy do reveal early adhesive differences between gold and PMS substrates favoring cytoskeletal-linked adhesion cluster formation. These initiate an interplay between clusters of MDCK II specific integrins in paxillin rich areas and e-cadherins at later culture stages up to 2 days of culture, where ECM is partially cast on PMS and the lifting of the cell sheet is already possible. Tight junctions could be identified after extended culture times when whole cell sheets were easily peeled off the substrate below LCST and the PMS retained the ECM component fibronectin while collagen I was lifted with the cells, possibly related to their stability against water loss. CP-AFM confirmed these adhesive differences between these two common ECM components. Cooperative behavior is thus visible on a very early time scale and on the molecular level up to the cellular level in crowded cultures facilitating collective cell-sheet production. This research methodology could also be applied to study the relationship between other cells and functional surfaces, ultimately helpful for designing effective cell culture surfaces in cell-sheet based tissue engineering.

MATERIALS AND METHODS

Synthesis of PNIPAm Microgel and Preparation of PMS. A solution of NIPAM (0.6 g) and BIS (0.04 g) were dissolved in deionized water (50 mL), and the solution was added to a three-necked flask equipped with a mechanical stirrer. Under stirring at 400 rpm, using a mechanical stirrer, the reaction medium was heated up to 70 °C. During this process, nitrogen was purged through the solution to remove oxygen. The reaction of polymerization was initiated by adding ammonium persulfate (APS, 0.03 g) and proceeded for 4 h. The reaction mixture was stirred overnight while cooling down to room temperature. The microgel solution was then distributed into individual centrifuge tubes and purified via centrifugation at 14 000 rpm and 15 °C for 30 min, followed by removal of the supernatant and resuspension with DI water. These steps were repeated for five times in order to remove unwanted side-products and residual reactants.

To prepare PMS, the glass part of IBIDI glass-bottom Petri dishes (μ-dish, 35 mm, Ibidi, Germany) were first coated with the help of an evaporation machine with 2 nm of titanium layer used to ensure adhesion of gold and then with a 15 nm thin gold film of RMS roughness below 1 nm to stabilize PMS. The monodispersed PNIPAm microgel solution is sonicated for 20 s to suspend the microgels on the Au/Ti coated glass substrate. A 30 μL portion of PNIPAm microgel solution was deposited on the Au/Ti coated glass substrate. The microgels are strongly attached on the gold surface noncovalently. The solution was allowed to dry completely over 20 min at 40 °C, by which a homogeneous microgel monolayer was assembled. The surface then rinsed several times with DI water to remove excess microgels not bound to the Au, and immersed in DI water at room temperature overnight while the DI water is changed every few hours.

AFM Measurement. *PNIPAm Characterization: QI Mode AFM Imaging and Determination of Young's Modulus.* Measurements were performed at different temperatures; 29 and 45 °C. Cantilevers (silicon nitride MSNL-10, Bruker, Germany, with a nominal spring constant of ≈0.01 N/m) were calibrated before each experiment with the thermal noise method.[78] An AFM (NanoWizard IV BioAFM, JPK, Berlin, Germany) with a Petri dish heater (Biocell, JPK Instrument AG, Berlin, Germany) mounted on an inverted optical microscope

https://dx.doi.org/10.1021/acsami.0c09166
ACS Appl. Mater. Interfaces 2020, 12, 33516−33529

(Olympus IX 81, Olympus, Japan) was operated in QI mode with an approach velocity in the range of 40 to 100 μm/s and set-point in range of 0.5−1.0 nN. After a temperature change, we waited 30 min for a new thermal equilibrium. The adhesive force is derived from the retrace part of the FD curves measured by QI mode AFM imaging for each single pixel of a scan line of the whole field of view on the PMS, and the minimum value of the FD curve represents the adhesion force for each measured point.

Quantitative analysis of acquired data was analyzed using the JPKSPM data processing software of the AFM manufacturer. The arithmetic average roughness, $R_a = 1/n\sum_i^n|y_i|$, where the surface contains n equally spaced points along the trace and y_i is the vertical distance from the mean line to the ith data point, is measured. To estimate the elasticity of the microgels, the indentation curves are fitted using the Sneddon model with a Biolodeau formula approximation as four-sided pyramid shape of cantilever probes are used: $F = 0.7453\frac{E}{(1-\upsilon^2)}\delta^2\cdot\tan\alpha$, where F, δ, E, υ, and α represent the loading force, the indentation depth, the local Young's modulus, the Poisson ratio (0.5), and half-opening angle of four-sided pyramidal indenter (15°), respectively.

Cell−Substrate and Cell−Cell Adhesion Using Single-Cell Adhesion Force Spectroscopy (SCFS). Adhesion strength to the PNIPAm decorated surface was quantified with an AFM-based SCFS setup combined with an optical microscope (AFM: CellHesion 200, JPK Instruments, Germany; Microscope: IX81, Olympus, Japan; Objective: 10xUPlanFL N/0.30/Ph1, or a 40× objective (1.35O∞/0.17/FM26.5, Olympus, Europe SE Co. KG), both with additional 1.6× magnification, Olympus Europe SE Co. KG; Camera: Orca Flash 2.8 C11440, Hamamatsu, Japan). We used tipless cantilevers (Arrow TL2-50, Nano World, Switzerland) with a resonance frequency of 6 kHz in liquid and a mean spring constant of 0.03 N/m. The spring constant was calibrated with the thermal noise method as mentioned above. After also testing more adhesive functionalizations like celltak and poly dopamine in the past, the cantilevers here were functionalized with poly-L-lysine (1 mg/mL, Sigma, P5899, −20 °C) showing the most satisfactory attachment efficiency for MDCK II cells. Therefore we followed this protocol: up to 5 mg is diluted in ultrapure H_2O (4 °C) to create 1 mL aliquot stock with a coating density efficiency of 4 $\mu g/cm^2$ on the cantilever. This is achieved by dipping the cantilever fixed to a holder in the poly-L-lysine solution for 1 h at room temperature and then, after removal, rinsing twice with ultrapure H_2O.

The gold coated IBIDI glass-bottom Petri dishes was coated with PNIPAm microgels as described above on one-half-side only, while the other half remained uncoated (Figure S5). Cells in serum-free HEPES buffered medium, otherwise comparable to culture medium, were allowed to seed and adhere for 15−30 min, before the measurement started. Several further measures were taken to avoid classical pitfalls of the SCFS method: To avoid adhesion adaptation and possible adhesion protein modulation due to continuous PMS exposure, we picked cells from the untreated (gold coated) part of the petri dish. Single cells were attached to the front of the cantilever under continuous optical control by picking them from the substrate thus allowing to establish adhesion to the cantilever during a time period of 2 min, thereby also ensuring for each single curve that the cell was not lost to the substrate but remained attached. Once a cell adhered to the tip, we measured cycles of approach and retraction resulting in a typical FD curve either toward two gold, PMS, or a lower cell, all on a new position the exclude influences of debris at the picking location.

In advance, SCFS parameters were optimized for measuring MDCK II cells: besides the functionalization mentioned above, we used an approach/retraction velocity of 2.5 μm/s to avoid hydrodynamic effects as well as cell rupture events, the smallest, minimally invasive contact force of 500 pN which still ensured successful approachment toward the surface and a contact time of 30 or 90 s to allow either cell−substrate or also cell−cell contact formation. After a relaxation time of 30 s to avoid adaptation to cycle experiments, we repeated the FD curve recording with the same parameter set for up to 5 times per cell and for usually 10 cells and 3 measurement days per category thus up to 50 FD curves each; see supplementary Table S6. The resulting FD curves were analyzed with the AFM manufactures software tool mentioned above, to extract the maximum adhesion force F_{max} and the integral between the FD curve and the baseline, thus representing the adhesion work W_{Adh}. In addition, we analyzed step features (instantaneous rupture events). The step parameters analyzed consist of the number of steps per curve, the step force, the length between two consecutive steps, the step slope, and the combined length until the last step, i.e., total detachment of the cell. During the experiments, a bright-field image was acquired for each measurement to ensure comparable radii of the cells and thus avoid big heterogeneity due to great differences in contact area and also to exclude multinucleated cells.

Colloidal Probe Force Spectroscopy. Measurements were performed in a cell medium environment (see above) at different temperatures of 29, 37, and 45 °C. Cantilevers (CP-PNPL-SiO-A, 2 μm SiO_2 colloidal particle) with nominal force constant of 0.08 N/m and a resonance frequency of 17 kHz were functionalized with ECM components of fibronectin (Sigma-Aldrich) and collagen I (Bovine, Gibco). The cantilevers were dipped in 50 μL of diluted fibronectin and collagen I solutions (1 mg/mL) for 30 min at room temperature. Functionalized cantilevers were calibrated before each experiment with thermal noise method. AFM instrument (NWIV, JPK BioAFM, Berlin, Germany) with a JPK petri dish heater mounted on an inverted optical microscope (Olympus IX 81) was operated in force spectroscopy mode with an approach and retraction velocity at 5 μm/s and set-point at 2.5 nN. The z-length of the piezo has a range of 15 μm. After the temperature switch, the setup was kept stationary for 30 min to find equilibrium. The acquired data was extracted using the python package jpkfile.[79] The baseline of the retraction curve was corrected with a linear fit and the minimum force was used to access the adhesion force using python.

Cell Culture. MDCK II cells (European Collection of Authenticated Cell Cultures) were maintained in minimum essential medium (Life Technologies) containing Earle's salts, 2.2 g/L $NaHCO_3$, 2 mM GlutaMAX and 10% fetal calf serum (FCS; BioWest), at 37 °C in a humidified incubator set to 5% CO_2. Cells were subcultured twice a week using Trypsin/EDTA (0.25%/0.02%; Biochrom).

Immunostaining. Cells were seeded on Au/Ti surface or PMS and cultivated for up to 1 week at 37 °C in a humidified incubator set to 5% CO_2. The resulting cell monolayer was rinsed with PBS (Biochrom) and fixed with 4% paraformaldehyde (PFA) in PBS for 20 min. To avoid unspecific binding of antibodies, the samples were treated with BSA (5% w/v in PBS) for 1 h. Staining was performed using the indicated primary antibodies for 1 h at room temperature followed by incubation for 1 h with the secondary antibody AlexaFluor 546 goat antimouse IgG (Thermo Fisher Scientific). The samples were rinsed three times with PBS after each step. Fluorescence micrographs were captured by means of confocal laser scanning microscopy (FluoView 1200, Olympus Europe SE Co. KG). The primary antibodies included fibronectin (Sigma-Aldrich, no. F7387), E-Cadherin Clone 36 (BD Transduction Laboratories, no. 610182), Collagen, Type I (Sigma-Aldrich, no. C2456), Paxillin Clone Y113 (Abcam, no. ab32084), and Alexa-Fluor488-conjugated ZO-1-1A12 (Thermo Fisher Scientific, no. 339188).

■ ASSOCIATED CONTENT

Supporting Information

The Supporting Information is available free of charge at https://pubs.acs.org/doi/10.1021/acsami.0c09166.

Supporting figures and tables. **Figure S1**. Optical images of PMS and bare gold surface. **Figure S2**. Qi-mode-imaging based 2D topology of microgels at 28 and 45 °C. **Figure S3**. Confocal images of fixated MDCK II cell sheet on gold substrate after 48 h. **Figure S4**. Contact angle measurement on the gold surface PMS and PMS

https://dx.doi.org/10.1021/acsami.0c09166
ACS Appl. Mater. Interfaces 2020, 12, 33516−33529

with remaining ECM after cell-sheet lift-off. **Figure S5**. Bright field images while conducting SCFS. **Figure S6.** Representative FD curves of SCFS. **Chapter S1.** Early cell−cell adhesion on PMS upon temperature changes monitored via SCFS. **Figure S7.** Cell−cell adhesion on bare gold and PMS upon temperature changes monitored via SCFS. **Figure S8.** Histogram of the probability distribution of slopes of each step. **Table S1**. F_{max}, W_{Adh}, F_{step}, step slope, l_{step}, N_{step}, and $l_{pulling}$ for SCFS. **Table S2**. Number of FD curves for step slope analysis. **Figure S9**. Ratio of jump steps to tether steps of MDCK II cells. **Table S3.** Correlation matrix for number of jump steps and tether steps. **Figure S10**. Average number of jump steps and tether steps of MDCK II cells. **Table S4**. Average number of jump and tether step in single FD curve. **Figure S11**. Confocal images of MDCK II cell-sheet culture on the gold substrate. **Figure S12**. Cell morphology at the early stage (6 h) of incubation. **Figure S13**. Results of SCFS with all results of significance tests. **Figure S14.** Interaction between ECM components and gold or PMS upon temperature switching. **Figure S15.** FD curves for the functionalized cantilevers. **Table S5.** Correlation matrix. **Table S6.** Number of measurement information of SCFS and CP-AFM (PDF)

AUTHOR INFORMATION

Corresponding Author

Marco Tarantola − *Max Planck Institute for Dynamics and Self Organization (MPIDS), 37077 Göttingen, Germany; Institute for Dynamics of Complex Systems, University of Göttingen, 37073 Göttingen, Germany;* orcid.org/0000-0002-1699-1019; Phone: +49-551-5176-316; Email: Marco.Tarantola@ds.mpg.de

Authors

Hyejeong Kim − *Max Planck Institute for Dynamics and Self Organization (MPIDS), 37077 Göttingen, Germany*

Hannes Witt − *Max Planck Institute for Dynamics and Self Organization (MPIDS), 37077 Göttingen, Germany*

Tabea A. Oswald − *Institute of Organic and Biomolecular Chemistry, University of Göttingen, 37077 Göttingen, Germany*

Complete contact information is available at: https://pubs.acs.org/10.1021/acsami.0c09166

Author Contributions

H.K. and M.T. designed the study. All authors participated in the experiments and data analysis in part or in whole; H.K. and M.T. worked on SCFS, H.K. and H.W. worked on QI-AFM and CP-AFM, and T.A.O. worked on confocal imaging. The manuscript was written through contributions of all authors. All authors have given approval to the final version of the manuscript.

Funding

We thank the Max Planck Society and the MPG fellow program, the Volkswagen Foundation Initiative LIFE (Project Living Foam) and SFB 937 "Collective behavior of soft and biological matter" (Project A8) for funding.

Notes

The authors declare no competing financial interest.

ACKNOWLEDGMENTS

We thank Katharina Gunkel, Maren-Stella Müller, and Angela Rübeling for their essential help in cantilever preparation and cell cultures, as well as Alexey Chizhik for the Ti/Au coated glass substrates. We are also very much indebted to Andreas Janshoff, Claudia Steinem, and Eberhard Bodenschatz for fruitful and lively discussions.

REFERENCES

(1) Yang, J.; Yamato, M.; Shimizu, T.; Sekine, H.; Ohashi, K.; Kanzaki, M.; Ohki, T.; Nishida, K.; Okano, T. Reconstruction of Functional Tissues with Cell Sheet Engineering. *Biomaterials* **2007**, *28* (34), 5033−5043.

(2) Ide, T.; Nishida, K.; Yamato, M.; Sumide, T.; Utsumi, M.; Nozaki, T.; Kikuchi, A.; Okano, T.; Tano, Y. Structural Characterization of Bioengineered Human Corneal Endothelial Cell Sheets Fabricated on Temperature-Responsive Culture Dishes. *Biomaterials* **2006**, *27* (4), 607−614.

(3) Li, M.; Ma, J.; Gao, Y.; Yang, L. Cell Sheet Technology: A Promising Strategy in Regenerative Medicine. *Cytotherapy* **2019**, *21* (1), 3−16.

(4) Guo, R.; Morimatsu, M.; Feng, T.; Lan, F.; Chang, D.; Wan, F.; Ling, Y. Stem Cell-Derived Cell Sheet Transplantation for Heart Tissue Repair in Myocardial Infarction. *Stem Cell Res. Ther.* **2020**, *11* (1), 19.

(5) Zhernenkov, M.; Ashkar, R.; Feng, H.; Akintewe, O. O.; Gallant, N. D.; Toomey, R.; Ankner, J. F.; Pynn, R. Thermoresponsive Pnipam Coatings on Nanostructured Gratings for Cell Alignment and Release. *ACS Appl. Mater. Interfaces* **2015**, *7* (22), 11857−11862.

(6) Tsai, H.-Y.; Vats, K.; Yates, M. Z.; Benoit, D. S. Two-Dimensional Patterns of Poly (N-Isopropylacrylamide) Microgels to Spatially Control Fibroblast Adhesion and Temperature-Responsive Detachment. *Langmuir* **2013**, *29* (39), 12183−12193.

(7) Xia, Y.; Tang, Y.; Wu, H.; Zhang, J.; Li, Z.; Pan, F.; Wang, S.; Wang, X.; Xu, H.; Lu, J. R. Fabrication of Patterned Thermoresponsive Microgel Strips on Cell-Adherent Background and Their Application for Cell Sheet Recovery. *ACS Appl. Mater. Interfaces* **2017**, *9* (2), 1255−1262.

(8) Nakao, M.; Kim, K.; Nagase, K.; Grainger, D. W.; Kanazawa, H.; Okano, T. Phenotypic Traits of Mesenchymal Stem Cell Sheets Fabricated by Temperature-Responsive Cell Culture Plate: Structural Characteristics of Msc Sheets. *Stem Cell Res. Ther.* **2019**, *10* (1), 1−14.

(9) Weder, G.; Guillaume-Gentil, O.; Matthey, N.; Montagne, F.; Heinzelmann, H.; Vörös, J.; Liley, M. The Quantification of Single Cell Adhesion on Functionalized Surfaces for Cell Sheet Engineering. *Biomaterials* **2010**, *31* (25), 6436−6443.

(10) Nishida, K.; Yamato, M.; Hayashida, Y.; Watanabe, K.; Yamamoto, K.; Adachi, E.; Nagai, S.; Kikuchi, A.; Maeda, N.; Watanabe, H.; et al. Corneal Reconstruction with Tissue-Engineered Cell Sheets Composed of Autologous Oral Mucosal Epithelium. *N. Engl. J. Med.* **2004**, *351* (12), 1187−1196.

(11) Nishida, K.; Yamato, M.; Hayashida, Y.; Watanabe, K.; Maeda, N.; Watanabe, H.; Yamamoto, K.; Nagai, S.; Kikuchi, A.; Tano, Y.; Okano, T. Functional Bioengineered Corneal Epithelial Sheet Grafts from Corneal Stem Cells Expanded Ex Vivo on a Temperature-Responsive Cell Culture Surface. *Transplantation* **2004**, *77* (3), 379−385.

(12) Kreis, C. T.; Grangier, A.; Bäumchen, O. In Vivo Adhesion Force Measurements of Chlamydomonas on Model Substrates. *Soft Matter* **2019**, *15* (14), 3027−3035.

(13) Doberenz, F.; Zeng, K.; Willems, C.; Zhang, K.; Groth, T. Thermoresponsive Polymers and Their Biomedical Application in Tissue Engineering. *J. Mater. Chem. B* **2020**, *8* (4), 607−628.

(14) Cooperstein, M. A.; Canavan, H. E. Biological Cell Detachment from Poly (N-Isopropyl Acrylamide) and Its Applications. *Langmuir* **2010**, *26* (11), 7695−7707.

(15) Heinen, S.; Cuéllar-Camacho, J. L.; Weinhart, M. Thermoresponsive Poly (Glycidyl Ether) Brushes on Gold: Surface Engineering Parameters and Their Implication for Cell Sheet Fabrication. *Acta Biomater.* **2017**, *59*, 117−128.
(16) Cooperstein, M. A.; Nguyen, P. A.; Canavan, H. E. Poly (N-Isopropyl Acrylamide)-Coated Surfaces: Investigation of the Mechanism of Cell Detachment. *Biointerphases* **2017**, *12* (2), 02C401.
(17) Engler, A. J.; Carag-Krieger, C.; Johnson, C. P.; Raab, M.; Tang, H.-Y.; Speicher, D. W.; Sanger, J. W.; Sanger, J. M.; Discher, D. E. Embryonic Cardiomyocytes Beat Best on a Matrix with Heart-Like Elasticity: Scar-Like Rigidity Inhibits Beating. *J. Cell Sci.* **2008**, *121* (22), 3794−3802.
(18) Rother, J.; Richter, C.; Turco, L.; Knoch, F.; Mey, I.; Luther, S.; Janshoff, A.; Bodenschatz, E.; Tarantola, M. Crosstalk of Cardiomyocytes and Fibroblasts in Co-Cultures. *Open Biol.* **2015**, *5* (6), 150038.
(19) Canavan, H. E.; Cheng, X.; Graham, D. J.; Ratner, B. D.; Castner, D. G. Cell Sheet Detachment Affects the Extracellular Matrix: A Surface Science Study Comparing Thermal Liftoff, Enzymatic, and Mechanical Methods. *J. Biomed. Mater. Res., Part A* **2005**, *75* (1), 1−13.
(20) Shimizu, T.; Yamato, M.; Isoi, Y.; Akutsu, T.; Setomaru, T.; Abe, K.; Kikuchi, A.; Umezu, M.; Okano, T. Fabrication of Pulsatile Cardiac Tissue Grafts Using a Novel 3-Dimensional Cell Sheet Manipulation Technique and Temperature-Responsive Cell Culture Surfaces. *Circ. Res.* **2002**, *90* (3), e40−e48.
(21) Yamato, M.; Utsumi, M.; Kushida, A.; Konno, C.; Kikuchi, A.; Okano, T. Thermo-Responsive Culture Dishes Allow the Intact Harvest of Multilayered Keratinocyte Sheets without Dispase by Reducing Temperature. *Tissue Eng.* **2001**, *7* (4), 473−480.
(22) Xia, Y.; He, X.; Cao, M.; Chen, C.; Xu, H.; Pan, F.; Lu, J. R. Thermoresponsive Microgel Films for Harvesting Cells and Cell Sheets. *Biomacromolecules* **2013**, *14* (10), 3615−3625.
(23) Kushida, A.; Yamato, M.; Kikuchi, A.; Okano, T. Two-Dimensional Manipulation of Differentiated Madin−Darby Canine Kidney (Mdck) Cell Sheets: The Noninvasive Harvest from Temperature-Responsive Culture Dishes and Transfer to Other Surfaces. *J. Biomed. Mater. Res.* **2001**, *54* (1), 37−46.
(24) Ermis, M.; Antmen, E.; Hasirci, V. Micro and Nanofabrication Methods to Control Cell-Substrate Interactions and Cell Behavior: A Review from the Tissue Engineering Perspective. *Bioactive materials* **2018**, *3* (3), 355−369.
(25) Kamprad, N.; Witt, H.; Schröder, M.; Kreis, C. T.; Bäumchen, O.; Janshoff, A.; Tarantola, M. Adhesion Strategies of Dictyostelium Discoideum−a Force Spectroscopy Study. *Nanoscale* **2018**, *10* (47), 22504−22519.
(26) Wei, J.; Cai, J.; Li, Y.; Wu, B.; Gong, X.; Ngai, T. Investigation of Cell Behaviors on Thermo-Responsive Pnipam Microgel Films. *Colloids Surf., B* **2015**, *132*, 202−207.
(27) Yoon, J. K.; Misra, M.; Yu, S. J.; Kim, H. Y.; Bhang, S. H.; Song, S. Y.; Lee, J. R.; Ryu, S.; Choo, Y. W.; Jeong, G. J.; et al. Thermosensitive, Stretchable, and Piezoelectric Substrate for Generation of Myogenic Cell Sheet Fragments from Human Mesenchymal Stem Cells for Skeletal Muscle Regeneration. *Adv. Funct. Mater.* **2017**, *27* (48), 1703853.
(28) Fan, Z.; Nie, Y.; Chen, Z.; Xie, X.; Liao, X.; Wei, Y. Construction of Novel Temperature-Responsive Hydrogel Culture System Based on the Biomimetic Method for Stem Cell Sheet Harvest. *J. Bioact. Compat. Polym.* **2019**, *34* (3), 229−245.
(29) Sanzari, I.; Buratti, E.; Huang, R.; Tusan, C. G.; Dinelli, F.; Evans, N. D.; Prodromakis, T.; Bertoldo, M. Poly (N-Isopropylacrylamide) Based Thin Microgel Films for Use in Cell Culture Applications. *Sci. Rep.* **2020**, DOI: 10.1038/s41598-020-63228-9.
(30) Yang, L.; Fan, X.; Zhang, J.; Ju, J. Preparation and Characterization of Thermoresponsive Poly (N-Isopropylacrylamide) for Cell Culture Applications. *Polymers* **2020**, *12* (2), 389.
(31) Switacz, V. K.; Wypysek, S. K.; Degen, R.; Crassous, J. J.; Spehr, M.; Richtering, W. Influence of Size and Cross-Linking Density of Microgels on Cellular Uptake and Uptake Kinetics. *Biomacromolecules* **2020**, DOI: 10.1021/acs.biomac.0c00478.
(32) Okano, T.; Yamada, N.; Okuhara, M.; Sakai, H.; Sakurai, Y. Mechanism of Cell Detachment from Temperature-Modulated, Hydrophilic-Hydrophobic Polymer Surfaces. *Biomaterials* **1995**, *16* (4), 297−303.
(33) Yamato, M.; Konno, C.; Kushida, A.; Hirose, M.; Utsumi, M.; Kikuchi, A.; Okano, T. Release of Adsorbed Fibronectin from Temperature-Responsive Culture Surfaces Requires Cellular Activity. *Biomaterials* **2000**, *21* (10), 981−986.
(34) Dai, W.; Zheng, C.; Zhao, B.; Chen, K.; Jia, P.; Yang, J.; Zhao, J. A Negative Correlation between Water Content and Protein Adsorption on Polymer Brushes. *J. Mater. Chem. B* **2019**, *7* (13), 2162−2168.
(35) Benoit, M.; Gabriel, D.; Gerisch, G.; Gaub, H. E. Discrete Interactions in Cell Adhesion Measured by Single-Molecule Force Spectroscopy. *Nat. Cell Biol.* **2000**, *2* (6), 313−317.
(36) Taubenberger, A.; Cisneros, D. A.; Friedrichs, J.; Puech, P.-H.; Muller, D. J.; Franz, C. M. Revealing Early Steps of A2β1 Integrin-Mediated Adhesion to Collagen Type I by Using Single-Cell Force Spectroscopy. *Mol. Biol. Cell* **2007**, *18* (5), 1634−1644.
(37) Drelich, J.; Mittal, K. L. *Atomic Force Microscopy in Adhesion Studies*; CRC Press: 2005.
(38) Khalili, A. A.; Ahmad, M. R. A Review of Cell Adhesion Studies for Biomedical and Biological Applications. *Int. J. Mol. Sci.* **2015**, *16* (8), 18149−18184.
(39) Schmidt, S.; Zeiser, M.; Hellweg, T.; Duschl, C.; Fery, A.; Möhwald, H. Adhesion and Mechanical Properties of Pnipam Microgel Films and Their Potential Use as Switchable Cell Culture Substrates. *Adv. Funct. Mater.* **2010**, *20* (19), 3235−3243.
(40) Uğur, Ş.; Elaissari, A.; Yargi, Ö.; Pekcan, Ö. Reversible Film Formation from Nano-Sized Pnipam Particles Below Glass Transition. *Colloid Polym. Sci.* **2006**, *285* (4), 423−430.
(41) Sackmann, E.; Smith, A.-S. Physics of Cell Adhesion: Some Lessons from Cell-Mimetic Systems. *Soft Matter* **2014**, *10* (11), 1644−1659.
(42) López-Colomé, A. M.; Lee-Rivera, I.; Benavides-Hidalgo, R.; López, E. Paxillin: A Crossroad in Pathological Cell Migration. *J. Hematol. Oncol.* **2017**, *10* (1), 1−15.
(43) Campbell, H. K.; Maiers, J. L.; DeMali, K. A. Interplay between Tight Junctions & Adherens Junctions. *Exp. Cell Res.* **2017**, *358* (1), 39−44.
(44) Sariisik, E.; Popov, C.; Müller, J. P.; Docheva, D.; Clausen-Schaumann, H.; Benoit, M. Decoding Cytoskeleton-Anchored and Non-Anchored Receptors from Single-Cell Adhesion Force Data. *Biophys. J.* **2015**, *109* (7), 1330−1333.
(45) Friedrichs, J.; Legate, K. R.; Schubert, R.; Bharadwaj, M.; Werner, C.; Müller, D. J.; Benoit, M. A Practical Guide to Quantify Cell Adhesion Using Single-Cell Force Spectroscopy. *Methods* **2013**, *60* (2), 169−178.
(46) Sackmann, E.; Merkel, R. *Lehrbuch Der Biophysik*; Wiley-VCH: 2009, Chapter 13.
(47) Zihni, C.; Mills, C.; Matter, K.; Balda, M. S. Tight Junctions: From Simple Barriers to Multifunctional Molecular Gates. *Nat. Rev. Mol. Cell Biol.* **2016**, *17* (9), 564.
(48) Singh, A. V.; Rahman, A.; Kumar, N. S.; Aditi, A.; Galluzzi, M.; Bovio, S.; Barozzi, S.; Montani, E.; Parazzoli, D. Bio-Inspired Approaches to Design Smart Fabrics. *Mater. Eng. (Reigate, U. K.)* **2012**, *36*, 829−839.
(49) Chung, T.-W.; Liu, D.-Z.; Wang, S.-Y.; Wang, S.-S. Enhancement of the Growth of Human Endothelial Cells by Surface Roughness at Nanometer Scale. *Biomaterials* **2003**, *24* (25), 4655−4661.
(50) Selhuber-Unkel, C.; López-García, M.; Kessler, H.; Spatz, J. P. Cooperativity in Adhesion Cluster Formation During Initial Cell Adhesion. *Biophys. J.* **2008**, *95* (11), 5424−5431.
(51) Kuznetsova, T. G.; Starodubtseva, M. N.; Yegorenkov, N. I.; Chizhik, S. A.; Zhdanov, R. I. Atomic Force Microscopy Probing of Cell Elasticity. *Micron* **2007**, *38* (8), 824−833.

(52) Gavara, N.; Chadwick, R. S. Determination of the Elastic Moduli of Thin Samples and Adherent Cells Using Conical Atomic Force Microscope Tips. *Nat. Nanotechnol.* **2012**, *7* (11), 733−736.
(53) Guo, Q.; Xia, Y.; Sandig, M.; Yang, J. Characterization of Cell Elasticity Correlated with Cell Morphology by Atomic Force Microscope. *J. Biomech.* **2012**, *45* (2), 304−309.
(54) Das, R. K.; Zouani, O. F. A Review of the Effects of the Cell Environment Physicochemical Nanoarchitecture on Stem Cell Commitment. *Biomaterials* **2014**, *35* (20), 5278−5293.
(55) Steltenkamp, S.; Rommel, C.; Wegener, J.; Janshoff, A. Membrane Stiffness of Animal Cells Challenged by Osmotic Stress. *Small* **2006**, *2* (8−9), 1016−1020.
(56) Vogler, E. A. Water and the Acute Biological Response to Surfaces. *J. Biomater. Sci., Polym. Ed.* **1999**, *10* (10), 1015−1045.
(57) Teräväinen, T. P.; Myllymäki, S. M.; Friedrichs, J.; Strohmeyer, N.; Moyano, J. V.; Wu, C.; Matlin, K. S.; Muller, D. J.; Manninen, A. Av-Integrins Are Required for Mechanotransduction in Mdck Epithelial Cells. *PLoS One* **2013**, *8* (8), e71485.
(58) Schoenenberger, C.-A.; Zuk, A.; Zinkl, G. M.; Kendall, D.; Matlin, K. S. Integrin Expression and Localization in Normal Mdck Cells and Transformed Mdck Cells Lacking Apical Polarity. *J. Cell Sci.* **1994**, *107* (2), 527−541.
(59) Myllymäki, S. M.; Teräväinen, T. P.; Manninen, A. Two Distinct Integrin-Mediated Mechanisms Contribute to Apical Lumen Formation in Epithelial Cells. *PLoS One* **2011**, *6* (5), e19453.
(60) Strohmeyer, N.; Bharadwaj, M.; Costell, M.; Fässler, R.; Müller, D. J. Fibronectin-Bound A5β1 Integrins Sense Load and Signal to Reinforce Adhesion in Less Than a Second. *Nat. Mater.* **2017**, *16* (12), 1262−1270.
(61) Delanoe-Ayari, H.; Al Kurdi, R.; Vallade, M.; Gulino-Debrac, D.; Riveline, D. Membrane and Acto-Myosin Tension Promote Clustering of Adhesion Proteins. *Proc. Natl. Acad. Sci. U. S. A.* **2004**, *101* (8), 2229−2234.
(62) Wu, Y.; Kanchanawong, P.; Zaidel-Bar, R. Actin-Delimited Adhesion-Independent Clustering of E-Cadherin Forms the Nanoscale Building Blocks of Adherens Junctions. *Dev. Cell* **2015**, *32* (2), 139−154.
(63) Fenz, S. F.; Bihr, T.; Schmidt, D.; Merkel, R.; Seifert, U.; Sengupta, K.; Smith, A.-S. Membrane Fluctuations Mediate Lateral Interaction between Cadherin Bonds. *Nat. Phys.* **2017**, *13* (9), 906−913.
(64) Panorchan, P.; Thompson, M. S.; Davis, K. J.; Tseng, Y.; Konstantopoulos, K.; Wirtz, D. Single-Molecule Analysis of Cadherin-Mediated Cell-Cell Adhesion. *J. Cell Sci.* **2006**, *119* (1), 66−74.
(65) Fichtner, D.; Lorenz, B.; Engin, S.; Deichmann, C.; Oelkers, M.; Janshoff, A.; Menke, A.; Wedlich, D.; Franz, C. M. Covalent and Density-Controlled Surface Immobilization of E-Cadherin for Adhesion Force Spectroscopy. *PLoS One* **2014**, *9* (3), e93123.
(66) Changede, R.; Sheetz, M. Integrin and Cadherin Clusters: A Robust Way to Organize Adhesions for Cell Mechanics. *BioEssays* **2017**, *39* (1), e201600123.
(67) Noethel, B.; Ramms, L.; Dreissen, G.; Hoffmann, M.; Springer, R.; Rübsam, M.; Ziegler, W. H.; Niessen, C. M.; Merkel, R.; Hoffmann, B. Transition of Responsive Mechanosensitive Elements from Focal Adhesions to Adherens Junctions on Epithelial Differentiation. *Mol. Biol. Cell* **2018**, *29* (19), 2317−2325.
(68) Shigetomi, K.; Ono, Y.; Inai, T.; Ikenouchi, J. Adherens Junctions Influence Tight Junction Formation Via Changes in Membrane Lipid Composition. *J. Cell Biol.* **2018**, *217* (7), 2373−2381.
(69) Brückner, B. R.; Janshoff, A. Importance of Integrity of Cell-Cell Junctions for the Mechanics of Confluent Mdck Ii Cells. *Sci. Rep.* **2018**, *8* (1), 1−11.
(70) Lin, J.-H.; Chang, H.-Y.; Kao, W.-L.; Lin, K.-Y.; Liao, H.-Y.; You, Y.-W.; Kuo, Y.-T.; Kuo, D.-Y.; Chu, K.-J.; Chu, Y.-H.; Shyue, J.-J. Effect of Surface Potential on Extracellular Matrix Protein Adsorption. *Langmuir* **2014**, *30* (34), 10328−10335.
(71) Karsch, S.; Kong, D.; Großhans, J.; Janshoff, A. Single-Cell Defects Cause a Long-Range Mechanical Response in a Confluent Epithelial Cell Layer. *Biophys. J.* **2017**, *113* (12), 2601−2608.
(72) Obert, E.; Strauss, R.; Brandon, C.; Grek, C.; Ghatnekar, G.; Gourdie, R.; Rohrer, B. Targeting the Tight Junction Protein, Zonula Occludens-1, with the Connexin43 Mimetic Peptide, Act1, Reduces Vegf-Dependent Rpe Pathophysiology. *J. Mol. Med.* **2017**, *95* (5), 535−552.
(73) Sancho, A.; Vandersmissen, I.; Craps, S.; Luttun, A.; Groll, J. A New Strategy to Measure Intercellular Adhesion Forces in Mature Cell-Cell Contacts. *Sci. Rep.* **2017**, *7*, 46152.
(74) Wysotzki, P.; Sancho, A.; Gimsa, J.; Groll, J. A Comparative Analysis of Detachment Forces and Energies in Initial and Mature Cell-Material Interaction. *Colloids Surf., B* **2020**, *190*, 110894.
(75) Nehls, S.; Nöding, H.; Karsch, S.; Ries, F.; Janshoff, A. Stiffness of Mdck Ii Cells Depends on Confluency and Cell Size. *Biophys. J.* **2019**, *116* (11), 2204−2211.
(76) Yu, M.; Strohmeyer, N.; Wang, J.; Müller, D. J.; Helenius, J. Increasing Throughput of Afm-Based Single Cell Adhesion Measurements through Multisubstrate Surfaces. *Beilstein J. Nanotechnol.* **2015**, *6* (1), 157−166.
(77) Dao, L.; Gonnermann, C.; Franz, C. M. Investigating Differential Cell-Matrix Adhesion by Directly Comparative Single-Cell Force Spectroscopy. *J. Mol. Recognit.* **2013**, *26* (11), 578−589.
(78) Hutter, J. L.; Bechhoefer, J. Calibration of Atomic-Force Microscope Tips. *Rev. Sci. Instrum.* **1993**, *64* (7), 1868−1873.
(79) Kuhlemann, I. *Jpkfile−a Python Module to Read Jpk File Formats*, version V1.3; 2019.

https://dx.doi.org/10.1021/acsami.0c09166
ACS Appl. Mater. Interfaces 2020, 12, 33516−33529